Spin-dependent reflection of very-low-energy electrons from W(110)

S. N. Samarin, J. F. Williams, and A. D. Sergeant
ARC Centre of Excellence for Antimatter-Matter Studies, University of Western Australia, Perth WA 6009, Australia

O. M. Artamonov
Research Institute of Physics, St. Petersburg University, St. Petersburg 199034, Russia

H. Gollisch and R. Feder
Theoretische Festkörperphysik, Universität Duisburg-Essen, D-47048 Duisburg, Germany
(Received 2 April 2007; revised manuscript received 9 August 2007; published 4 September 2007)

For spin-polarized electrons in the energy range of 8–21 eV incident off-normally on a W(110) surface, we have measured the energy distribution of secondary electrons using a time-of-flight technique and a position-sensitive detector. Selecting the elastically scattered electrons in the specular direction, we obtained the spin asymmetry of the (00) low-energy electron diffraction beam as a function of the primary electron energy and incidence angle. Calculations on the basis of a relativistic multiple scattering formalism, with potential input derived from the self-consistently calculated ground state electronic structure, yielded (00) beam spectra in rather good agreement with their experimental counterparts. In particular, we found a prominent asymmetry feature of about 60% slightly below the emergence threshold energy for two nonspecular beams. Its physical origin is a region of strong spin-orbit coupling between even and odd bulk states, but its size, sign, and energy depend sensitively on the surface potential barrier, which identifies it as a surface resonance. Experimentally, the surface sensitivity of the large asymmetry is revealed by its sign reversal after oxygen exposure.

DOI: 10.1103/PhysRevB.76.125402 PACS number(s): 79.20.Hx, 61.14.Hg, 71.70.Ej, 73.20.At

I. INTRODUCTION

Elastic and inelastic scattering of spin-polarized low-energy electrons from a solid surface are largely used for studying spin-dependent electron scattering dynamics, the spin-dependent electronic structure of ferromagnetic surfaces, magnetic surface excitations, and also the geometrical surface structure (cf. Refs. 1–3, and references therein). For a nonmagnetic surface, the spin effect in elastic scattering is due to the spin-orbit interaction, which is strongest for high-Z materials such as Pb, Au, and W. Tungsten is the ideal model target, since its surface can be prepared and cleaned in a reproducible way that allows for a comparison of results obtained by different methods. It has been studied by most of the surface science techniques providing, together with corresponding theoretical work, rather complete information on the electronic and geometric structures of the surface.

Spin-polarized low-energy electron diffraction (SPLEED) from W(001) has been studied extensively both experimentally and theoretically.[4,5] Even a spin detector based on SPLEED from W(001) was developed.[6,7] Much less is known about SPLEED from the (110) surface of W. Polarization analysis of the (00) beam from W(110) was successfully used to determine the surface structure by means of rotation curves.[8] To the best of our knowledge, there was only one measurement of the intensity asymmetry of the (00) beam from W(110) as a function of the primary energy using spin-polarized incident electrons.[9] In the two last-mentioned experiments, the energy was in the range from 30 to 100 eV.

On the other hand, the spin-dependent reflectivity of electrons in the range of energies below 20 eV is very interesting and important for several reasons.

(i) Surface resonances at energies just below the emergence of new diffracted beams are observed as low-energy electron diffraction (LEED) fine structures (cf. review Refs. 10 and 11). They arise from multiple scattering of electrons between the topmost atomic layer and the surface potential barrier. These resonances have mainly been studied with unpolarized incident electrons.[12] The extension of these measurements to a polarized incident beam allows insight into the spin dependence of surface resonances.

(ii) The surface potential barrier on metals plays a prominent role in very-low-energy electron scattering. The knowledge of its shape is very important in the proper description of phenomena such as adsorption of atoms on the surface, secondary emission, photoelectron emission, and the contact potential between two metals. For the determination of the surface barrier on W(001) and W(110), the measurements of fine structure profiles in very-low-energy electron diffraction have been performed successfully.[13] Adding a new variable, spin, in such measurements provides additional information for theoreticians for an adequate description of the scattering experiment and the surface potential barrier itself.[14–17]

(iii) The fine structure in angle-resolved secondary electron spectra has been shown theoretically[18] and experimentally (cf. Ref. 19, and references therein) to replicate in detail the fine structure in corresponding LEED spectra. For nonnormal emission, spin-orbit coupling has been theoretically predicted to produce spin polarization of the emitted electrons.[18] The intensity asymmetry in secondary emission from W(110) excited by spin-polarized electrons was observed experimentally.[20] The interpretation of the spin-polarized secondary emission spectroscopy can be related to the SPLEED measurements in the corresponding energy range.

(iv) The spin-dependent reflectivity of low-energy electrons is directly related to the spin-dependent electron transmission through the surface into the crystal. At the experimental conditions, when the reflectivity shows a high spin

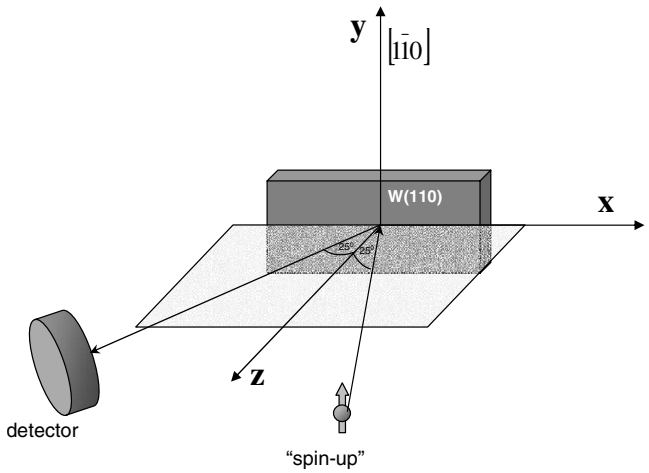

FIG. 1. Geometry of the experiment.

asymmetry, the surface works like a "polarization filter" for electrons. Knowledge of these conditions provides an opportunity for the "spin injection" into the crystal using unpolarized electrons. This effect might be relevant to the spintronic devices, where the spin injection is one of the important issues.

In this paper, we present a joint experimental and theoretical investigation of the intensity asymmetry of the specular reflection of spin-polarized electrons from a W(110) surface in the energy range of 8–21 eV.

II. EXPERIMENTAL DETAILS

We measured the intensity asymmetry of electrons elastically scattered from the W(110) surface under diffraction conditions in specular geometry [(00) diffraction beam] for spin-polarized primary electrons with energy from 8 to 21 eV. The energy distributions of inelastically scattered electrons were also measured. The measurements have been carried out at various incidence and detection angles as described below.

The experiments were performed in UHV conditions, with the base pressure in the 10^{-11} Torr range. The W(110) crystal was mounted on a rotatable manipulator in such a way that the [1$\bar{1}$0] direction was along the rotational axis and perpendicular to the scattering plane that contains the normal to the sample surface and the detector (Fig. 1).

The sample was cleaned in vacuum using a standard procedure[21] including oxygen treatment at 10^{-7} Torr oxygen pressure and 1400 K sample temperature, followed by a few high-temperature flashes up to 2300 K. The cleanliness of the surface was monitored by Auger electron spectroscopy and low-energy electron diffraction as well as by two-electron coincidence spectroscopy, which is very sensitive to the presence of oxygen.[22] The angle between the incident electron beam and the axis of the detector, as shown in Fig. 1, is $\alpha+\beta=50°$. We used a time-of-flight technique for electron energy measurements.[23] The incident electron beam is pulsed with a pulse width less than 1 ns to have a reference point on a time scale. Scattered and ejected electrons are detected by a position-sensitive detector based on 75 mm diameter microchannel plates. The flight distance from the sample to the center of the detector is 126 mm. Position sensitivity of the detector allows the flight distance correction for electrons arriving at different positions on the detector.

The energy resolution of this technique depends on the electron energy: it is better for slow electrons than for fast electrons. It can be estimated by a half-width of 0.5 eV for 13 eV elastic maximum. The spin-polarized electron gun is based on photoemission from a strained GaAs crystal activated by Cs and oxygen adsorption.[24] Photoelectrons excited by a circularly polarized light from a diode laser with the wavelength of 836 nm are initially longitudinally polarized. They pass through a 90° deflector such that the emergent beam is now transversely polarized. The polarization P of the electron beam was measured to be $66\pm2\%$ in two separate experiments. One includes the measurements of P_3 Stokes parameter on atomic neon, and the second, measurements of the known asymmetry of Stoner excitations on a ferromagnetic surface. It can be reversed from P to $-P$ by changing the sense of circular polarization of the laser light incident on the GaAs photocathode. The degree of polarization is rather stable during measurement time, which was confirmed by repeatedly performed measurements of the scattering asymmetry. For a given primary energy and fixed experimental geometry, the energy distribution curves of secondary electrons are measured for spin-up (I^u) and spin-down (I^d) polarizations of the incident beam, and then these two spectra are compared in terms of spin asymmetry, which is defined as $A=(I^u-I^d)/(I^u+I^d)$. To avoid the influence of the incident electron current drift or the sample surface contamination on the spin asymmetry during the measurements, the polarization of the beam was reversed every 5 s.

We used the position sensitivity of the detector to select only electrons that scattered coherently and formed a diffraction pattern. Figure 2(a) represents a three-dimensional (3D) image of the (00) diffraction pattern on the detector. Figure 2(b) shows the projection of this image on the x coordinate of the detector. The black rectangle on the figure indicates the selected area of the detector, which is assigned to the diffraction spot. The rectangle crosses the projection at about half of its height. Such a selection provides reasonable statistics for the diffraction peak and cuts out nonspecularly scattered electrons. The gray cylinder in Fig. 2(a) indicates the 3D representation of this selected area. One can see that the cylinder embraces almost the entire peak. Figure 2(c) presents an image of the (00) diffraction pattern on the detector in a logarithmic intensity gray scale for $\alpha=\beta=25°$ and primary energy 13 eV. The white circle shows the selected area (inside the circle), which we assigned to the diffraction spot. It means that we can effectively choose the acceptance angle of detection by selecting a certain area on the detector. The experimental data on SPLEED asymmetry presented in this paper are calculated using scattering intensities inside the selection circle. We note here that the selection of elastically scattered electrons inside this circle increases the measured intensity asymmetry. In the inelastic part of the spectrum, the intensity asymmetry even changes the sign when we change the selection from inside to outside the circle.

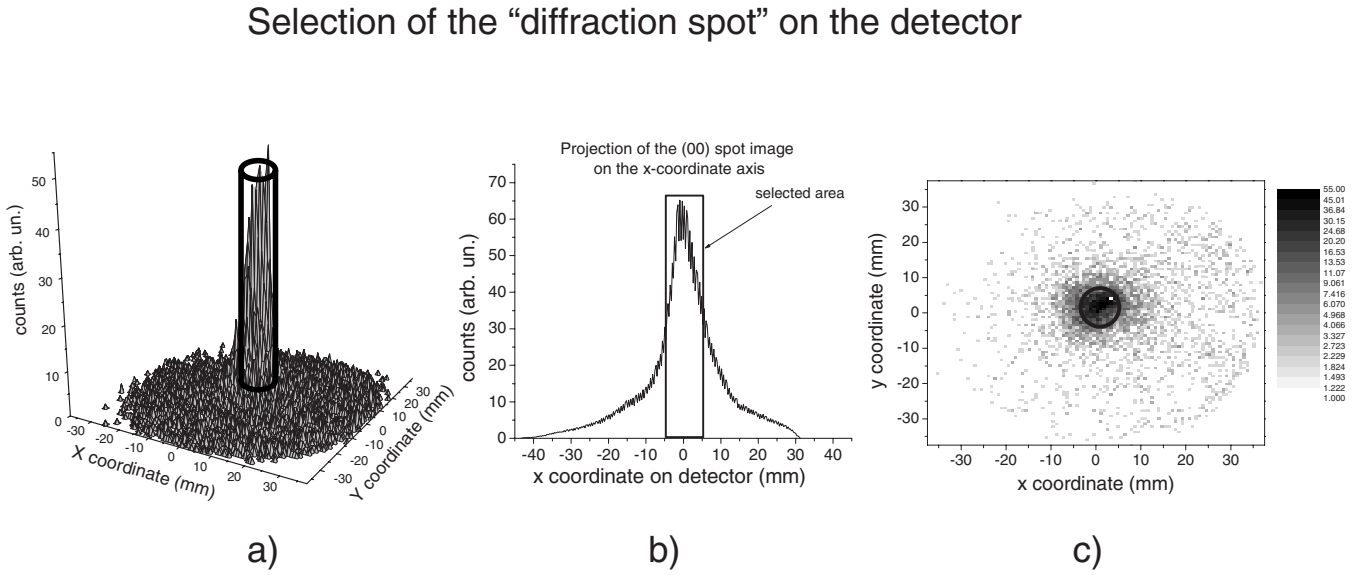

FIG. 2. (a) 3D image of the diffraction spot on the position-sensitive detector; gray cylinder represents the selected area assigned to the diffraction spot. (b) Projection of the diffraction spot image on the x coordinate of the detector; the black rectangle shows the selected area of the diffraction spot. (c) Image of the (00) diffraction pattern on the detector in a logarithmic intensity gray scale; the white circle shows the selected area (inside the circle), which is assigned to the diffraction spot.

This part of the spectrum is not discussed in the paper because it is not within the scope of the paper. The energy-dependent reflectivity of the elastic scattering for spin-up and spin-down electrons was not measured because we could not control reliably the incident electron current, which varies as a function of energy.

III. THEORETICAL APPROACH

Spin-dependent LEED intensity spectra and the corresponding spin-orbit-induced asymmetry spectra from W(110) have been calculated by means of a relativistic layer Korringa-Kohn-Rostoker code (cf. Refs. 1 and 25). In view of further interpreting individual features of these spectra, the same code was employed to obtain bulk band structures without and with spin-orbit coupling. In the following, we specify the geometry and the effective one-electron potential, which we have used as input for the above calculations. Special attention is paid to the surface potential barrier, since it plays an important role in determining, via multiple scattering, the asymmetry features, which we have observed experimentally.

As one would expect for a close-packed surface, W(110) is not reconstructed except for a possible slight relaxation of the topmost atomic layer. While earlier LEED analyses suggest no such relaxation, more recent studies using LEED intensity spectra,[26,27] SPLEED rotation diagrams,[8] and photoelectron diffraction[28] agree with each other that the topmost interlayer spacing is reduced by about 3% with respect to the bulk value. This is also supported by first-principles calculations.[26] We, therefore, choose in our calculations an inward relaxation of 3%.

For the purpose of constructing the quasiparticle potential input for our SPLEED calculations, we computed the electronic structure of the ground state of a nine-layer W(110) slab with the above surface geometry within density functional theory by means of the full-potential linearized augmented plane wave program package WIEN2K (Ref. 29) using a local density approximation for the exchange-correlation energy. The thus obtained potential was cast into muffin form.

For the quasiparticle potential in the bulk region, we use the resulting layer-dependent spherically symmetric potential parts and the constant real inner potential augmented by a spatially uniform complex self-energy correction. The imaginary part V_{0i} of the latter was taken from previous LEED experience as $-0.1(E+\phi)^{0.83}$ eV, where E denotes the incident electron energy and ϕ the work function, which for W(110) is $\phi=5$ eV. For the real part of the self-energy correction, a constant of 1 eV (yielding a real inner potential of 15.85 eV) turned out to be acceptable for matching our present experimental data.

The surface potential barrier, strictly speaking, involves an energy-dependent complex nonlocal electronic self-energy term. From this one may derive an effective local form felt by quasielectrons (cf., e.g., Ref. 30, and references therein). For our present purpose, it suffices, however, to adopt a local model form with adjustable parameters, the initial choice of which is guided by the near-surface form of the ground state surface potential barrier. In contrast to the latter, this model form has the asymptotic image behavior and can simulate dynamic effects (in particular, energy dependence). For its real part $V_r(z)$, we take the following special case of a model previously used for LEED.[31] Placing the crystal in the half-space $z>0$ with the topmost internuclear plane at $z=0$, $V_r(z)$ has (in a.u.) the image form $1/[4(z-z_1)]$ for $z<z_2=2z_1<z_1<0$, where z_1 and $z_2=2z_1$ specify an image potential plane and a matching plane, respectively. For $z_2<z<0$, $V_r(z)$ is a third-order polynomial such that it

matches, up to the first derivative, the real inner potential at $z=0$ and the image potential form at z_2. Choosing $z_1=-2.7$ bohr and, hence, $z_2=-5.4$ bohr, $V_r(z)$ is found to closely reproduce the surface-parallel average $V_0(z)$ of our first-principles ground state potential in the near-surface region. For comparison, we note that the truncated bulk surface (jellium edge) is at $z=-2.1$ bohr. Farther outside, $V_r(z)$ has the physically correct image form instead of the exponential decay, which our ground state potential has due to the locality of the exchange-correlation approximation used in its calculation.

For the excited-state one-electron energies in LEED, the above $V_r(z)$ is modified by dynamical effects: first, there is the already mentioned reduction of the real part of the inner potential, which also affects $V_r(z)$, and second, the barrier moves inward, which is classically plausible from the retardation of the image charge. The best fit with our experimental asymmetry data was obtained for the image plane position $z_1=-1.8$ bohr (and hence, $z_2=-3.6$ bohr) instead of the ground state value $z_1=-2.7$ bohr.

The imaginary part $V_i(z)$ of the barrier is chosen as V_{0i} for $z_1<z<0$, where V_{0i} is the above-defined absorptive part of the inner potential, and as $\exp[-a(z-z_1)^2]$ for $z<z_1$, with $a=0.07$ found suitable for attaining agreement with our SPLEED asymmetry data.

The above smooth surface potential barrier model first refracts beams, which are incident from the vacuum and from the bulk crystal side, and second, reflects these beams, with characteristic amplitude reflection coefficients. These reflections, leading, in particular, to multiple scattering between surface barrier and bulk, are responsible for drastic surface barrier effects in LEED. To identify surface barrier effects in observed LEED spectra, it is, therefore, useful to consider, in addition to the realistic surface barrier model, a very simple model: a hypothetical step barrier (a potential jump from zero to the constant real inner potential, located at the edge of the truncated bulk) which still refracts incident beams but which does not reflect them at all. In short, this simple model is commonly referred to as a refracting but nonreflecting step barrier.

IV. RESULTS AND DISCUSSION

We measured energy distribution curves for a set of primary energies from 8 to 21 eV with increments of 0.5 eV in specular geometry with the incidence angle $\beta=(25\pm2)°$, i.e., $\alpha=\beta=:\theta$, where θ is the polar angle notation usual in the definition of spherical harmonics and in LEED work. For each primary energy, the elastically scattered electrons were selected inside the white circle of Fig. 2, and the asymmetry was calculated and normalized to our primary beam polarization of $66\pm2\%$. The thus determined asymmetry is plotted as a function of the primary electron energy E in Fig. 3(a). It shows a resonancelike energy dependence with a maximum of $60\pm3\%$ at $E=(12.5\pm0.5)$ eV and a minimum of $-33\pm3\%$ at $E=14\pm0.5$ eV.

To explore the surface sensitivity of the asymmetry spectrum, we adsorbed oxygen with an exposure of about 5 L at 1400 K. We observed, at 100 eV, a LEED pattern with clear half-order spots suggestive of a $p(2\times2)$ structure. From detailed studies of oxygen chemisorption on W(110) (cf., e.g., Refs. 32 and 33, and references therein), on the one hand, and from having an overall coverage of about 0.3.–0.4 ML, on the other hand, we conclude, however, that we have is-

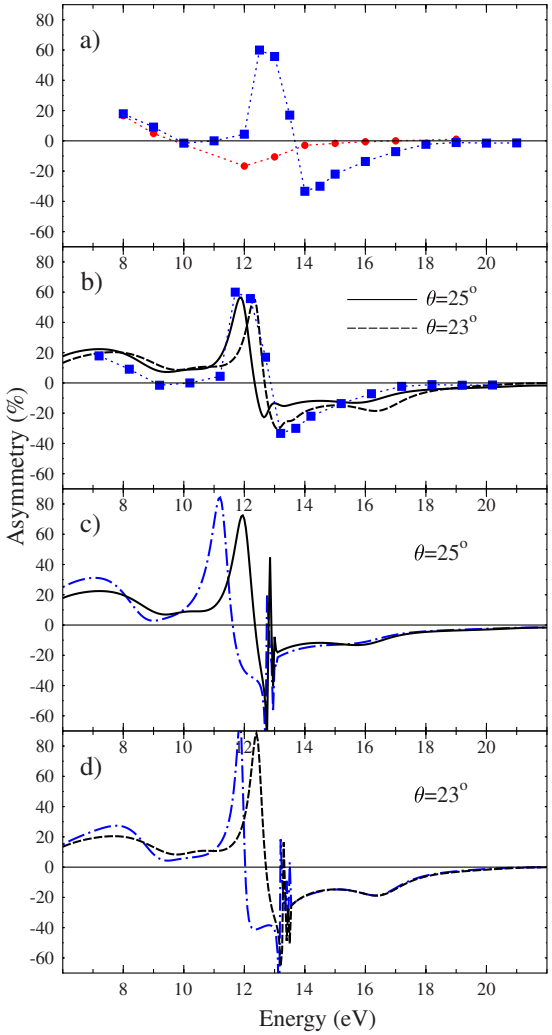

FIG. 3. (Color online) SPLEED intensity asymmetry $A(E)$ of the (00) beam from W(110). The scattering plane is the ΓPN plane; i.e., the surface projection of the wave vector $\vec{k}$ is along the [001] direction. (a) Experiment for polar angle of incidence $\theta=25\pm2°$ for the clean surface [blue (gray) squares] and an oxygen-covered one [red (gray) dots]. The experimental uncertainty of A is given by the height of the squares. (The dotted lines connecting the squares and the dots are to guide the eye.) (b) Theoretical $A(E)$ for $\theta=25°$ (solid black line) and $\theta=23°$ (dashed black line): obtained for a smooth surface barrier (as defined in Sec. III) with image plane position $z_1=-1.8$, from calculated spin-up and spin-down intensities which have been convoluted with a Gaussian of 0.4 eV FWHM. The blue (gray) squares represent the experimental $A(E)$ shifted by 0.8 eV toward lower energy. (The dotted line connecting the squares is to guide the eye.) (c) Theoretical $A(E)$ for $\theta=25°$ for surface barrier with $z_1=-1.8$ (solid black line) and $z_1=-2.7$ [dash-dotted blue (gray) line]. (d) Theoretical $A(E)$ for $\theta=23°$ for surface barrier with $z_1=-1.8$ (dashed black line) and $z_1=-2.7$ [dash-dotted blue (gray) line].

lands of 2×1 domains with probable contribution of 2×2 domains. With this oxygen coverage on W(110), we obtained the second asymmetry curve shown in Fig. 3(a). Compared to the asymmetry for clean W(110), it is smaller and has the opposite sign at the energies of the main peak. The asymmetry is, thus, seen to be very surface sensitive.

In Fig. 3(b), we show theoretical $A(E)$ spectra for clean W(110) for angles $\theta=25°$ and 23°, which were obtained from calculated spin-up and spin-down intensities convoluted by a Gaussian of 0.4 eV full width at half maximum (FWHM). Bearing in mind the uncertainty of ±2° in our absolute angular measurements and the angular spread of about 1° of the primary beam, the calculated asymmetry is in rather good agreement with our experimental data if the latter are shifted by 0.8 eV toward lower energy, which is within the accuracy of the absolute energy calibration in the experiment.

The corresponding original (not convoluted) theoretical $A(E)$ for $\theta=25°$ is shown as the solid curve in Fig. 3(c). It was obtained using the smooth surface barrier model described in Sec. III, with the image plane position parameter $z_1=-1.8$. While the main peak at 11.8 eV is just somewhat higher than in Fig. 3(b), a series of very sharp resonances appears at around 13 eV. Noting that at 13.04 eV there is the threshold of emergence of two nonspecular beams into the vacuum region, these features are identified as the asymmetry correlates of the well-known surface resonances in spin-dependent LEED intensity spectra (Refs. 14–16, and references therein). To demonstrate the sensitivity of $A(E)$ to the key parameter z_1 of our smooth surface barrier model with image asymptotics, we show in Fig. 3(c) also $A(E)$ calculated for $z_1=-2.7$, i.e., the value obtained as an initial choice by fitting our first-principles ground state potential in the near-surface region. Compared to $A(E)$ for $z_1=-1.8$, the resonances get nonlinearly spread out, with the main peak displaced by about 0.7 eV toward lower energy. Hence, its convoluted counterpart moves by about 0.7 eV further away from the experimental peak [cf. Fig. 3(b)]. This indicates that the barrier with the image plane position parameter $z_1=-1.8$ is clearly favorable. The preference for the position $z_1=-1.8$ over $z_1=-2.7$ is plausible, since retardation in the formation of the image charge moves the barrier closer to the topmost atomic layer with increasing energy.

Analogous surface resonances are obtained for $\theta=23°$, for which the beam emergence threshold energy is 13.48 eV [Fig. 3(d)].

Now we explore in more detail the physical origin of the asymmetry spectra shown in Fig. 3. As is well known (cf., e.g., Ref. 1, and references therein), spin polarization and asymmetry in LEED from nonmagnetic solids are a consequence of spin-orbit coupling (SOC). Further, LEED intensity spectra are known to be closely linked to the bulk band structure in the corresponding energy range (cf., e.g., Refs. 34 and 35, and references therein). We have, therefore, investigated the links between SOC-induced features of the bulk band structure and our above SPLEED asymmetry spectra. The results are demonstrated by means of Fig. 4.

In Fig. 4(a), we show $E(k_z;k\sin\theta)$, with $k=(2E)^{1/2}$ and $\theta=25°$, calculated scalar relativistically, i.e., without SOC, for the real bulk muffin-tin potential. Since the scattering plane is a mirror plane of the crystal, the bulk eigenstates belonging to these bands are either even (labeled by "g") or odd (labeled by "u") with respect to reflection at this plane. SOC hybridizes even and odd states and produces gaps in the band structure ("avoided crossings") [see Fig. 4(b)], which we marked with red (gray) circles.

If the imaginary part of the potential is taken into account, k_z becomes complex. Instead of showing $E(\mathrm{Im}\,k_z)$ explicitly, we incorporate some essential information on it in a plot of $E(\mathrm{Re}\,k_z)$ [see Fig. 4(c)] by the following color (gray scale) coding: black if $\mathrm{Im}\,k_z<0.2$ and green (gray) if $\mathrm{Im}\,k_z>0.2$. The weakly damped black parts are seen [in Fig. 4(c)] to correspond quite closely to the real-potential bands [in Fig. 4(b)] except for changes near the critical points, which become inflection points of the complex-potential band structure.

Proceeding to LEED intensity and asymmetry spectra, we first consider the spectra obtained from a truncated bulk crystal (without surface relaxation) with a refracting but nonreflecting step barrier (cf. Sec. III), since these are more closely linked to the bulk band structure than the spectra for a reflecting barrier like the realistic smooth one described in Sec. III. The relation between LEED intensity spectra for a nonreflecting step barrier and the band structure (of symmetry character such that coupling to plane waves on the vacuum side is possible) is briefly such that peaks are associated with a low density of states (DOS), especially with band gaps, and minima with a high DOS. Details and further references may be found in Refs. 34 and 35. In the present case of off-normal incidence in a mirror plane, the relevant Bloch wave parts are those of even character. The spin-up and spin-down intensity spectra $I^+(E)$ and $I^-(E)$ in Fig. 4(d), which were obtained for the nonreflecting step barrier, basically obey the relationship described above while differing in detail from each other due to SOC. Of particular interest is the almost-zero minimum of $I^+(E)$ at 11.35 eV, since it is associated with a large negative asymmetry feature [cf. Fig. 4(e)]. At this energy there is not only a high density of states due to the even band ending at 11.3 eV (in the real-potential band structure), which by itself would entail no reflection, but also a lower density of states in the even-odd hybridization region [marked in Figs. 4(b) and 4(c) by the circle around $(E,\mathrm{Re}\,k_z)=(10.7,0.6)$], which apparently produces a small spin-dependent reflection.

Still using the nonreflecting step barrier, but replacing the truncated bulk model by the more realistic W(110) model with a 3% inward relaxation and layer-dependent ion-core potentials (cf. Sec. III), one obtains almost the same intensity and asymmetry curves as the ones shown in Figs. 4(d) and 4(e), but shifted by about 0.8 eV toward higher energy.

If, however, we employ—instead of the nonreflecting step barrier—the realistic reflecting smooth barrier with image asymptotics (cf. Sec. III) (with the image plane parameter $z_1=-1.8$ determined by comparison with our experimental data), we obtain spectra [Figs. 4(f) and 4(g)] which are drastically different at energies below the emergence threshold of two nonspecular beams at 13.04 eV. The spin-dependent intensities exhibit surface resonances, which translate them-

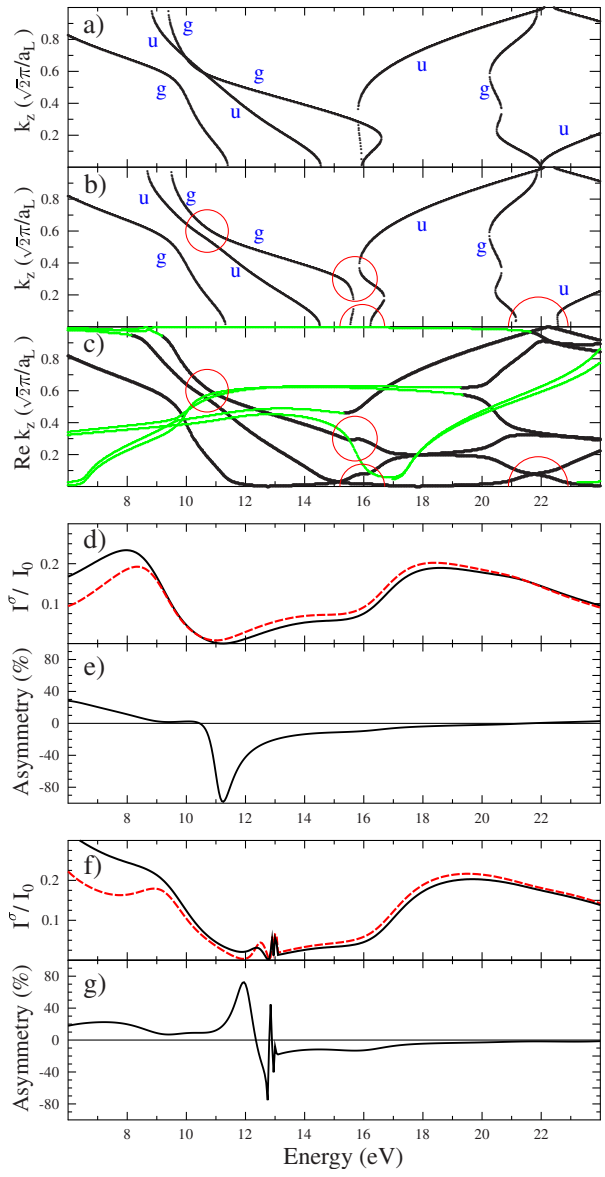

FIG. 4. (Color online) Band structure and SPLEED from W(110) for polar angle $\theta=25°$. (a) Scalar relativistic (without SOC) band structure $E(k_z)$ for real potential. a_L denotes the lattice constant of W. The labels g (u) refer to the even (odd) symmetry of the states with respect to reflection at the scattering plane. (b) Fully relativistic (with SOC) band structure $E(k_z)$ for real potential. The labels g (u) indicate the symmetry of the predominant part in the spin-orbit-hybridized states. Regions of strong hybridization are indicated by red (gray) circles. (c) Fully relativistic (with SOC) band structure $E(\mathrm{Re}\,k_z)$ for complex (quasiparticle) potential with imaginary part −0.5 eV. Parts of the bands for which $\mathrm{Im}\,k_z<0.2$ ($\mathrm{Im}\,k_z>0.2$) are represented by black [green (gray)] lines. (d) Spin-dependent intensities I^+ (solid black curve) and I^- [dashed red (gray) curve] of the 00 beam (relative to the primary beam intensity I_0) obtained for the truncated bulk structure (without surface relaxation) with the refracting but nonreflecting step barrier model (cf. Sec. III). (e) Asymmetry of the intensities shown in (d). (f) Same as (d) but calculated for the contracted topmost interlayer spacing (cf. Sec. III), layer-dependent ion-core potentials and the smooth surface barrier model (cf. Sec. III) with image plane parameter $z_1=-1.8$. (g) Asymmetry of the intensities shown in (f).

selves into resonances in the asymmetry $A(E)$ [which is identical to the solid $A(E)$ curve shown in Fig. 3(c)]. Most notably, we retrieve the experimentally observed big positive asymmetry feature instead of the big negative feature, which was obtained for the nonreflecting step barrier. The physical origin of the positive asymmetry feature is, thus, elucidated. Its very existence is due to spin-orbit hybridization between even and odd bulk quasiparticle states, but its sign and precise energy are determined by multiple scattering between the topmost atomic layer and the surface potential barrier.

Attempts aiming at a quantitative explanation of the $A(E)$ spectrum measured for our oxygen-covered W(110) surface [cf. Fig. 3(a)] seem not warranted for the following reasons. They would require first-principles calculations of electronic and geometric surface structures, which are very demanding, as well as an extension of our present SPLEED computer code to handle the more complicated potential in the surface region. (Approaches to LEED from metal surfaces with chemisorbed oxygen may, e.g., be found in Ref. 36, and references therein.) Moreover, our experimental $A(E)$ involves contributions from domains of different structures with poorly known relative weights.

For a fixed primary energy of 13 eV, we measured the angular dependence of the (00) beam asymmetry in the angular range $\alpha=\beta=:\theta=20°-30°$. This angular range was scanned by rotating the sample and selecting the specular diffraction spot on the detector. This range is limited by the size of the detector: within this angular range, the specular beam is still visible on the detector. The result of the measurements is presented in Fig. 5(a). It shows a maximum at $\theta=25°$ and goes to zero at $\theta=21°$. As was mentioned above, there is an uncertainty of ±2° in the absolute angular measurements that is related to the determination of the incidence angle $\beta=0$. On the other hand, the relative angular measurements that are shown in Fig. 5(a) are more precise (±0.5°).

Theoretical $A(\theta)$ and $I(\theta)$ results, which we calculated at energies 11.8, 12.0, and 12.2 eV using the smooth surface barrier with the image plane located at $z_1=-1.8$, which we found suitable for reproducing our experimental $A(E)$ data (cf. Fig. 3), are presented in Figs. 5(c) and 5(d). The angular dependence is, like the energy dependence, characterized by surface resonances, which now occur below the emergence threshold angles for the respective energies.

To make contact with our experimental data, we calculated a "broadened asymmetry" $A_b(\theta)$ in the following way. Denoting by $I^\sigma(E;\theta)$, with $\sigma=\pm$, spin-dependent intensities calculated as functions of E and θ, we formed the broadened intensities

$$I_b^\sigma(\theta)=\int dE'\,d\theta'\,G(E',E=12\ \mathrm{eV})G(\theta',\theta)I^\sigma(E';\theta'),$$

where $G(E',E=12\ \mathrm{eV})$ is a Gaussian of FWHM 0.4 eV and $G(\theta',\theta)$ is a Gaussian of angular FWHM 1° accounting for the experimental relative angular uncertainty. The resulting broadened asymmetry $A_b(\theta)=[I_b^+(\theta)-I_b^-(\theta)]/[I_b^+(\theta)+I_b^-(\theta)]$ is shown in Fig. 5(b). Except for the single experimental data point at $\theta=23°$, it is seen to compare fairly well with the

experimental $A(\theta)$ shifted to the left by 0.8°, which is well within the uncertainty in our absolute angle measurement.

V. CONCLUSION

Using a time-of-flight technique and a position-sensitive detector, we have measured—as a function of energy and incidence angle—the intensity asymmetry of electrons elastically reflected from the W(110) surface for spin-polarized primary electrons with energy from 8 to 21 eV. In particular, we observed an asymmetry versus energy spectrum, which is dominated by a large feature of about +60% slightly below the emergence threshold for nonspecular beams. The surface sensitivity of this asymmetry peak is proven by submonolayer oxygen adsorption, upon which it reverses its sign.

In order to understand our experimental data, we calculated spin-dependent LEED intensity spectra and the corresponding asymmetry spectra by means of a relativistic multiple scattering formalism. The choice of the potential input for these calculations, in particular, the surface potential barrier, was guided by a self-consistently calculated ground state electronic structure and augmented to incorporate quasiparticle effects. Using a smooth surface barrier, the image plane of which is about 1 bohr closer to the topmost atomic layer than that of the ground-state-derived barrier, we obtained rather good agreement with our experimental asymmetry curves.

In particular, we reproduced the observed asymmetry peak of about +60% below a nonspecular beam emergence threshold. By comparing with calculated band structures without and with SOC, this feature can be associated with a region of strong SOC between bulk quasiparticle states of even and odd mirror symmetries. Auxiliary LEED calculations with a refracting but nonreflecting step barrier, which are directly related to the bulk band structure, produced, however, a large negative asymmetry, in contrast to the calculations with the smooth reflecting barrier model. The observed dominant asymmetry feature is thereby clearly identified as a surface resonance, which is, as some further calculations corroborated, very sensitive to details of the surface potential barrier. In contrast, the spin-dependent intensity and asymmetry spectra above the beam emergence threshold are almost the same for the various surface barriers.

SPLEED surface resonances like the one reported in this work should manifest themselves in spin-polarized secondary emission spectra and be of use in the interpretation of the latter because of the close connection between LEED and secondary electron emission (cf. Refs. 18 and 19, and references therein). In fact, the asymmetry of the energy distribution curve of secondary electrons from W(110) excited by 25.5 eV spin-polarized electrons at 12° off-normal incidence exhibits a broad maximum in the energy range of 12–14 eV.[20] A similar result has been observed for normal electron incidence on W(110) with primary energies from 22 to 26 eV and scattering plane parallel to the ΓPN plane of the Brillouin zone,[37] where a maximum of the asymmetry in the secondary electron distributions shows up around 13 eV.

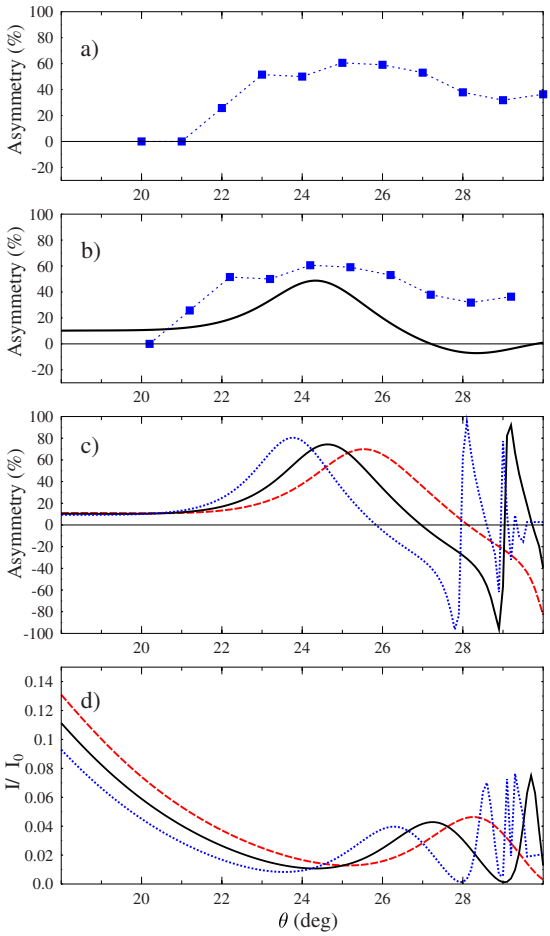

FIG. 5. (Color online) SPLEED spectra of the (00) beam from W(110) as functions of the polar angle of incidence θ. (a) Experimental asymmetry $A(\theta)$ for energy $E=13$ eV. The experimental uncertainty of A is given by the height of the squares. (b) Theoretical asymmetry $A_b(\theta)$ obtained by Gaussian convolutions as described in the text. The blue (gray) squares represent the experimental $A(\theta)$ shifted by 0.8° toward smaller angles. (c) Theoretical asymmetry spectra $A(\theta)$ for energies 11.8 eV [dashed red (gray) line], 12.0 eV (solid black line), and 12.2 eV [dotted blue (gray) line]. (d) Same (c), but spin-averaged intensity spectra $I(\theta)$.

The occurrence of strong resonancelike spin asymmetries in SPLEED, like the one reported in this work, also has implications for designing or interpreting spin-resolved photoemission and $(e,2e)$ experiments, in which the final state consists of one or two time-reversed LEED states. If one is interested in initial state properties or in electron-electron scattering dynamics, one should avoid conditions giving rise to surface resonances, since they are likely to obscure the quantities one intends to study.

Finally, we would like to mention a potential relevance of our results for spintronics. Since a strong spin dependence of the reflectivity of low-energy electrons implies spin-selective transmission into the crystal, knowledge of the experimental conditions when it occurs may be useful for designing devices with spin injection by means of unpolarized electrons.

[1] *Polarized Electrons in Surface Physics*, edited by R. Feder (World Scientific, Singapore, 1985).
[2] J. Kirschner, *Polarized Electrons at Surfaces*, Springer Tracts in Modern Physics Vol. 106 (Springer, Heidelberg, 1958).
[3] J. Henk, in *Handbook of Thin Film Materials*, edited by H. S. Nalwa (Academic, San Diego, 2001), Vol. 2, pp. 479–526.
[4] R. Feder and J. Kirschner, Surf. Sci. **103**, 75 (1981).
[5] R. Feder, J. Phys. C **14**, 2049 (1981).
[6] J. Kirschner and R. Feder, Phys. Rev. Lett. **42**, 1008 (1979).
[7] J. Sawler and D. Venus, Rev. Sci. Instrum. **62**, 2409 (1991).
[8] D. Venus, S. Cool, and M. Plihal, Surf. Sci. **446**, 199 (2000).
[9] G. Waller and U. Gradmann, Phys. Rev. B **26**, 6330 (1982).
[10] E. G. McRae, Rev. Mod. Phys. **51**, 541 (1979).
[11] R. O. Jones and P. J. Jennings, Surf. Sci. Rep. **9**, 165 (1988).
[12] J.-M. Baribeau and D. Roy, Surf. Sci. **166**, 234 (1986).
[13] J.-M. Baribeau, J. Lopez, and J.-C. Le Boss, J. Phys. C **18**, 3083 (1985).
[14] E. G. McRae, D. T. Pierce, G. C. Wang, and R. J. Celotta, Phys. Rev. B **24**, 4230 (1981).
[15] R. O. Jones and P. J. Jennings, Phys. Rev. B **27**, 4702 (1983).
[16] E. Tamura and R. Feder, Solid State Commun. **58**, 729 (1986).
[17] J. W. Krewer, W. Duerr, D. Pescia, and R. Feder, Solid State Commun. **74**, 137 (1990).
[18] R. Feder and J. B. Pendry, Solid State Commun. **26**, 519 (1978).
[19] M. Bovet, V. N. Strocov, F. Clerc, C. Koitzsch, D. Naumovic, and P. Aebi, Phys. Rev. Lett. **93**, 107601 (2004).
[20] S. N. Samarin, O. M. Artamonov, A. D. Sergeant, and J. F. Williams, Surf. Sci. **579**, 166 (2005).
[21] R. Cortenraada, S. N. Ermolov, V. N. Semenov, A. W. Denier van der Gon, V. G. Glebovsky, S. I. Bozhko, and H. H. Brongersma, J. Cryst. Growth **222**, 154 (2001).
[22] S. Samarin, J. Berakdar, R. Herrmann, H. Schwabe, O. Artamonov, and J. Kirschner, J. Phys. IV **9**, Pr6-137 (1999).
[23] S. N. Samarin, O. M. Artamonov, D. K. Waterhouse, J. Kirschner, A. Morozov, and J. F. Williams, Rev. Sci. Instrum. **74**, 1274 (2003).
[24] D. T. Pierce, R. J. Celotta, G.-C. Wang, W. N. Unertl, A. Galejs, C. E. Kuyatt, and S. R. Mielczarek, Rev. Sci. Instrum. **51**, 478 (1980).
[25] S. V. Halilov, E. Tamura, H. Gollisch, D. Meinert, and R. Feder, J. Phys.: Condens. Matter **5**, 3859 (1993).
[26] M. Arnold, K. Heinz, and M. Scheffler, Surf. Sci. **382**, 288 (1997).
[27] G. Teeter, J. L. Erskine, F. Shi, and M. A. Van Hove, Phys. Rev. B **60**, 1975 (1999).
[28] H. L. Meyerheim, D. Sander, R. Popescu, P. Steadman, S. Ferrer, and J. Kirschner, Surf. Sci. **475**, 103 (2001).
[29] P. Blaha, K. Schwarz, G. K. H. Madsen, D. Kvasnicka, and J. Luitz, WIEN2K, An Augmented Plane Wave Plus Local Orbitals Program for Calculating Crystal Properties, Vienna University of Technology, Austria, 2001.
[30] I. D. White, R. W. Godby, M. M. Rieger, and R. J. Needs, Phys. Rev. Lett. **80**, 4265 (1998).
[31] J. Rundgren and G. Malmstroem, J. Phys. C **10**, 4677 (1977).
[32] P. K. Wu, M. C. Tringides, and M. G. Lagally, Phys. Rev. B **39**, 7595 (1989).
[33] D. M. Riffe and G. K. Wertheim, Surf. Sci. **399**, 248 (1998).
[34] J. B. Pendry, *Low Energy Electron Diffraction* (Academic, New York, 1974).
[35] V. N. Strocov, Int. J. Mod. Phys. B **9**, 1755 (1995).
[36] Chang Q. Sun and Chunli Bai, J. Phys.: Condens. Matter **9**, 5823 (1997).
[37] S. N. Samarin, O. M. Artamonov, A. D. Sergeant, and J. F. Williams (unpublished).